The effect of the geometric factor on the *V-I* curve of Tl2212 film

2001 J. Phys.: Condens. Matter 13 6509

(http://iopscience.iop.org/0953-8984/13/30/306)

INSTITUTE OF PHYSICS PUBLISHING JOURNAL OF PHYSICS: CONDENSED MATTER

J. Phys.: Condens. Matter **13** (2001) 6509–6518 PII: S0953-8984(01)25071-1

The effect of the geometric factor on the V–I curve of Tl2212 film

S Y Ding[1], **Y Liu, X F Wu, F Y Lin, Z H Wang and L Qiu**

Department of Physics and National Laboratory of Solid State Microstructures, Nanjing University, Nanjing 210093, People's Republic of China

E-mail: syding@netra.nju.edu.cn (S Y Ding)

Received 21 May 2001
Published 13 July 2001
Online at stacks.iop.org/JPhysCM/13/6509

Abstract

A numerical procedure is proposed for calculating the current density j and electric field E from measurements of the electric transport inside a sample with rectangular cross section by solving the non-linear electric field diffusion equation based upon the collective creep model. It is shown that the sample geometry greatly affects E and j and thus the V–I curve. To verify our numerical prediction, the V–I curve and critical current of $Tl_2Ba_2CaCu_2O_{8+x}$ films with a rectangular cross section in various magnetic fields and temperatures were measured. Comparison shows that the numerical results agree well with the experimental data.

1. Introduction

Electron transport measurement plays a key role in the characterization of type II superconductivity of classical superconductors [1]. Resistance-broadening experiments on high-temperature superconductors have greatly enriched our knowledge of the properties of the mixed state [2–8]. Measurement of the V–I characteristic curve is also important for understanding vortex physics and vortex matter [9–11]. In attempts to understand the V–I characteristics, one of the assumptions widely adopted up to now is that the current is homogeneous in superconductors. On this assumption, a measured V–I curve can be changed directly to the E–j one, on the basis of which a variety of vortex properties have been studied and understood. Nevertheless, there are difficulties in explaining some of the experiments in terms of homogeneous current distribution. For example, it is found that the V–I curve of Ag-sheathed Bi-2223 tapes depends on the sweep rate of the applied current ($\mathrm{d}I/\mathrm{d}t$) [12]. It has also been reported that the resistance of $YBa_2Cu_3O_{7-\delta}$ films decays with time, i.e. the resistance relaxes [13]. It has been pointed out that these experiments can be understood if one assumes that current in the sample is spatially inhomogeneous [14,15]. The underlying physics

[1] Author to whom any correspondence should be addressed.

0953-8984/01/306509+10$30.00

is giant flux creep in a sample caused by small flux pinning barriers coupled with high operating temperatures. In a V–I curve experiment, an applied current always penetrates the measured sample from its surfaces and then diffuses into its inner part with a certain diffusion speed (v). The larger the rate $\mathrm{d}I/\mathrm{d}t$, the higher the current density and the electric field near the sample surfaces. It is possible that $\mathrm{d}I/\mathrm{d}t$ is so large compared with v that a detectable electric field at the outer part of the sample has already been induced due to the current diffusion, while there is almost no current in the inner part. That is to say, the current density j is inhomogeneous during the application of the current. Moreover, the inhomogeneity of j may lead to an electric field comparable to the experimental criterion of the critical current I_c when the applied current I in the sample is far smaller than I_c. There is a similar situation for a sample in an applied magnetic field, i.e. the magnetic shielding current density is dependent on the sweep rate of the applied field. In magnetic relaxation experiments, the initial magnetization differs with different sweep rates of the applied field [16, 17]. In such experiments, the irreversible magnetization ΔM at a given field H is dependent on the sweep rate $\mathrm{d}H/\mathrm{d}t$. The higher $\mathrm{d}H/\mathrm{d}t$, the larger ΔM [18, 19]. In ac susceptibility experiments, the higher the ac field frequency, the higher the peak of the imaginary part of the ac susceptibility [20, 21].

It has been shown that the geometry of a sample affects the distributions of the flux density B and the electric field E when magnetic relaxation is conducted without [22] and with flux creep [23]. It is expected that the sample geometry should influence the transport current diffusion when a current is applied [24]. Unfortunately, simulations such as those in references [14, 15] are carried out only for the simplest sample shape, a one-dimensional sample, while samples in real experiments may be more complicated. It is not clear what the influence of geometry would be on E and j and thus V–I measurements [24].

In this paper we report a numerical calculation of the V–I curves of a sample with rectangular cross section based upon the collective flux creep model. It is found that the sample geometry affects the V–I curve since it affects the inhomogeneous distribution of E and j. To solve the two-dimensional non-linear diffusion equation and observe numerically the space and time evolution of E and j, and the corresponding V–I curve, a procedure is proposed. The characteristic V–I curves of a $Tl_2Ba_2CaCu_2O_{8+x}$ (Tl2212) sample with rectangular cross section at different temperatures and fields have been measured and compared to the calculated V–I ones.

2. Experimental procedure

A 200 nm thick rectangular Tl2212 ($Tl_2Ba_2CaCu_2O_{8+x}$) film (8×12 mm^2) was deposited on a (001) $SrTiO_3$ single-crystal substrate by dc magnetron sputtering and four hours of post-annealing at 750 °C from a pair of Tl2212 superconductor targets which were prepared by solid-state reaction of stoichiometric amounts of Ca, BaO, CuO and Tl_2O_3 powders. Then, the rectangular film was photolithographically etched as a bridge of length $l = 0.1$ mm and cross section $S = 30\ \mu\mathrm{m} \times 0.2\ \mu\mathrm{m}$, as shown schematically in figure 1(a). Examination of the four metal atoms shows the composition to be 2.1Tl:2.0Ba:1.0Ca:1.9Cu. Details of the growth process of the film can be found in reference [25]. Four-terminal contact points of silver were used to measure the V–I and R–T curves. The onset transition temperature T_c was 103.2 K, with a 10%–90% width less than 1 K according to the R–T curve.

The V–I characteristic curves of the film as displayed in figure 2 were measured at different parallel fields and temperatures. The angle between the magnetic field and the film was less than 0.2°, so the influence of the orientation of the field could be neglected. It is obvious that the critical current I_{c0} is a function of temperature T and applied field H. In our calculation, we define I_{c0} at a certain reference voltage $V_0 = 10\ \mu\mathrm{V}$.

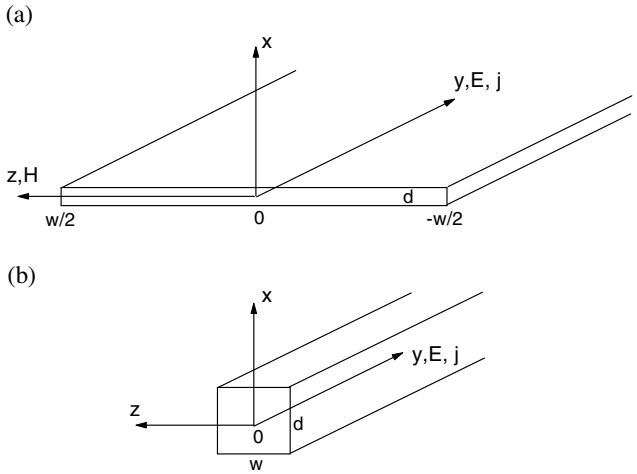

Figure 1. Samples with rectangular cross section. The applied current is in the y-direction; d = thickness, w = width. (a) $d \ll w$, for our Tl2212 film. (b) $d = w$.

It has been mentioned above that in the V–I curve measurement, j and E may be non-homogeneous when the current has not penetrated the sample, so the spatially inhomogeneous j and E will give rise to $(\mathrm{d}I/\mathrm{d}t)$-dependent V–I curves [12–15]. By plotting the log–log V–I curves it is also shown that most of these curves consist of two parts. In the part with large current, where the current has penetrated throughout the sample, the V–I characteristic can be well fitted in terms of a power-law relationship:

$$V = V_0\left(\frac{I}{I_{c0}}\right)^n \tag{1}$$

whence the parameter n is easily obtained. Moreover, one can safely assume that in this part, j and E are uniform inside the sample (see figure 5, later). Consequently, equation (1) is equivalent to

$$E = E_0\left(\frac{j}{j_{c0}}\right)^n \tag{2a}$$

where $E_0 = V_0/l = 0.1\ \mathrm{V\ m^{-1}}$, $j_{c0} = I_{c0}/S$.

Generally speaking, the $E(j)$ relation cannot be obtained just from the V–I characteristic, for the former describes a local property while the latter reflects an average one. However, equation (2a) indicates that the $E(j)$ relation can be described by the collective creep model of vortex glass with the glass exponent $\mu = 0$. The physical meanings of j_{c0} and E_0 can be seen if one assumes that the effective barrier of flux creep is logarithmic, $U(T, H, j) = U_0(T, H)\ln(j_{c0}/j)$, and the induced electric field of thermally activated flux hopping is just equation (2a) according to $E = vB = \nu_0 \mathrm{e}^{-U/(kT)}B$, with $n = U_0(T, H)/(kT)$ and $E_0 = \nu_0 B$, where v and v_0 are flux speeds with and without barriers.

In addition, there are other reasons leading the simulation of the power-law behaviour. Experimentally, the measurement of local magnetic relaxation in high-temperature superconductors with a Hall probe array shows that the dependence of the local activation energy U on time has the same form [26, 27]. Theoretically, from a very general point of view the dynamical behaviour of the critical state in a type II superconductor provides an example of self-organized criticality. The dynamical behaviour then tends to eliminate all the fluctuations in the system such that the relaxation rate and hence $U(j)$ become constant throughout the

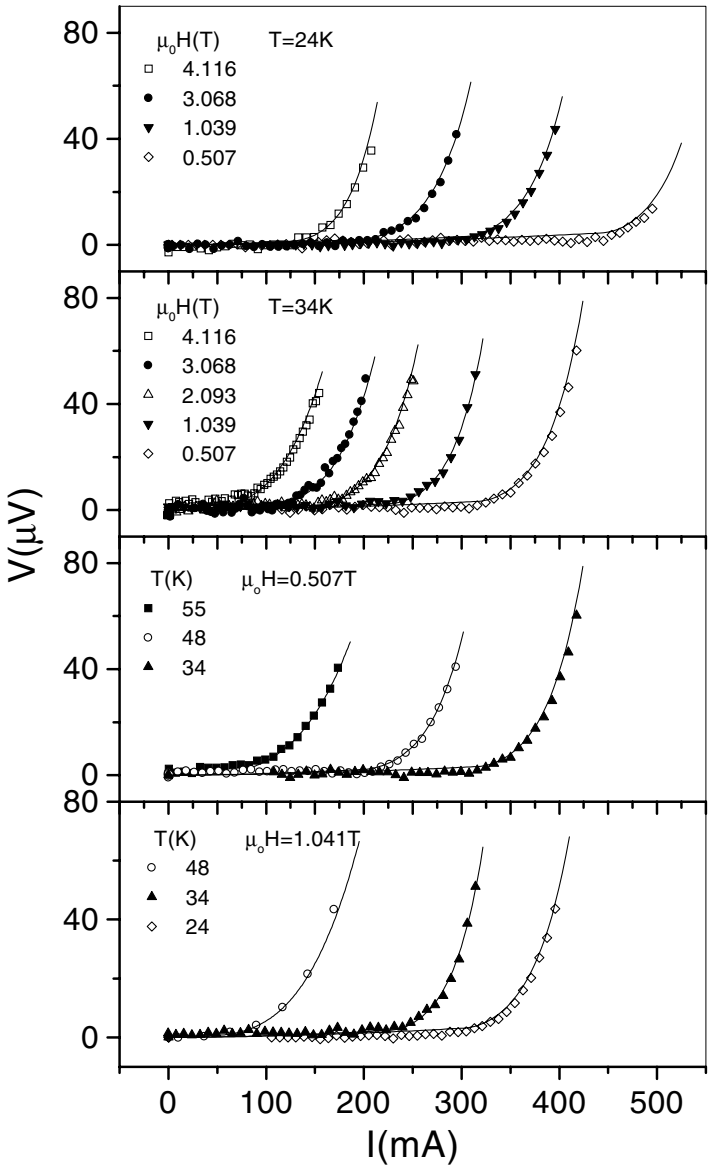

Figure 2. V–I characteristics of Tl2212 film at different applied fields H and temperatures T. The symbols represent the experimental data and the lines numerical results.

sample [11]. It is thus very natural to assume that the relationship between U and j mentioned above will still be correct on a local scale—as well as the power-law relationship described in equation (2a). Hence, we can write equation (2a) in another form:

$$E(x, z, t) = E_0 \left[\frac{j(x, z, t)}{j_{c0}} \right]^n \tag{2b}$$

where, in general, E_0, n and j_{c0} are functions of temperature and magnetic field, respectively. In the next section, equation (2b) will act as a material equation for conducting calculations.

3. Numerical calculation

3.1. Basic equations

Let us consider the bridge as a strip of infinite length along the y-axis, thickness d along the x-axis and width w along the z-axis (see figure 1) When the current is applied along the y-axis, the electric field and current density have only y-components $E(x, z, t)$ and $j(x, z, t)$, respectively, while the rotating flux density $\vec{B}$ has x- and z-components. According to the Maxwell equations $\partial\vec{B}/\partial t = -\vec{\nabla} \times \vec{E}$ and $\vec{\nabla} \times \vec{B} = \mu_0\vec{j}$, the diffusion equation for E is given by

$$\mu_0 \frac{\partial j(x, z, t)}{\partial t} = \left(\frac{\partial^2}{\partial x^2} + \frac{\partial^2}{\partial z^2}\right) E(x, z, t). \tag{3a}$$

The V–I experiment has shown that the electric field induced by the current-density change rate is described by equation (2b). It is pointed out that equation (2b) can describe not only the non-linear flux creep such as in Tl2212 film with $1 < n < \infty$, but also the ohmic behaviour, for which $n = 1$, and the Bean critical state, $n \to \infty$. Substituting equation (2b) into (3a) yields the electric field diffusion equation

$$\frac{\partial E}{\partial t} = \frac{nE_0^{1/n}}{\mu_0 j_{c0}} E^{1-1/n} \left(\frac{\partial^2}{\partial x^2} + \frac{\partial^2}{\partial z^2}\right) E. \tag{3b}$$

One can also obtain the diffusion equations for j or B in the same way [11, 16–19, 22–24]. However, we found that it is more correct to determine the boundary conditions for solving equation (3b) numerically (see the next section). In particular, when $d \ll w$, the two-dimensional equation is reduced to an infinite slab whose diffusion equation for E is one dimensional:

$$\frac{\partial E}{\partial t} = \frac{nE_0^{1/n}}{\mu_0 j_{c0}} E^{1-1/n} \frac{\partial^2 E}{\partial x^2}.$$

3.2. The boundary and initial conditions

3.2.1. The V–I curve at zero applied field. In a V–I curve measurement, the current is always applied with a certain sweep rate $\mathrm{d}I/\mathrm{d}t$. The boundary condition of equation (3b) can be obtained from the current conservation equation:

$$\frac{\partial}{\partial t} \int_0^w \int_0^d j \, \mathrm{d}x \, \mathrm{d}z = \frac{\mathrm{d}I}{\mathrm{d}t}.$$

Substituting equation (3a) into the conservation equation we obtain

$$\mu_0 \frac{\partial}{\partial t} \int_0^w \int_0^d j \, \mathrm{d}x \, \mathrm{d}z = \int_0^w \mathrm{d}z \int_0^d \frac{\partial^2 E}{\partial x^2} \, \mathrm{d}x + \int_0^d \mathrm{d}x \int_0^w \frac{\partial^2 E}{\partial z^2} \, \mathrm{d}z = \mu_0 \frac{\mathrm{d}I}{\mathrm{d}t}.$$

By symmetry, we have

$$\left.\frac{\partial E}{\partial x}\right|_{x=0} = -\left.\frac{\partial E}{\partial x}\right|_{x=d} \qquad \left.\frac{\partial E}{\partial z}\right|_{z=0} = -\left.\frac{\partial E}{\partial z}\right|_{z=w}.$$

Thus, the first boundary condition is simply given by

$$\int_0^w \left.\frac{\partial E}{\partial x}\right|_{x=0} \mathrm{d}z + \int_0^d \left.\frac{\partial E}{\partial z}\right|_{z=0} \mathrm{d}x = -\frac{\mu_0}{2} \frac{\mathrm{d}I}{\mathrm{d}t}. \tag{4a}$$

Furthermore, in the centre of the sample $B|_{x=d/2} = B|_{z=w/2} \equiv 0$, so the second boundary condition is

$$\left.\frac{\partial E}{\partial x}\right|_{x=d/2} = -\left.\frac{\partial B_z}{\partial t}\right|_{x=d/2} = 0 \qquad \left.\frac{\partial E}{\partial z}\right|_{z=w/2} = \left.\frac{\partial B_x}{\partial t}\right|_{z=w/2} = 0. \tag{5a}$$

As for the initial condition, there is no electric field in the sample at $t = 0$; that is,

$$E(x, z, t)\big|_{t=0} = 0. \tag{6}$$

3.2.2. The magnetization curve with zero applied current. It is easy to see that for magnetic measurement of, for example, the hysteresis loop or relaxation, there is no applied current:

$$\frac{\partial}{\partial t}\int_0^w \int_0^d j \, \mathrm{d}x \, \mathrm{d}z = 0.$$

Substituting equation (3) into the current conservation equation, we obtain

$$\mu_0 \frac{\partial}{\partial t}\int_0^w \int_0^d j \, \mathrm{d}x \, \mathrm{d}z = \int_0^w \mathrm{d}z \int_0^d \frac{\partial^2 E}{\partial x^2} \, \mathrm{d}x + \int_0^d \mathrm{d}x \int_0^w \frac{\partial^2 E}{\partial z^2} \, \mathrm{d}z = 0.$$

For anti-symmetry, we have

$$\left.\frac{\partial E}{\partial x}\right|_{x=0} = \left.\frac{\partial E}{\partial x}\right|_{x=d} \qquad \left.\frac{\partial E}{\partial z}\right|_{z=0} = \left.\frac{\partial E}{\partial z}\right|_{z=w}.$$

Thus, the first boundary condition in the magnetic measurement is

$$\int_0^w \left.\frac{\partial E}{\partial x}\right|_{x=0} \mathrm{d}z + \int_0^d \left.\frac{\partial E}{\partial z}\right|_{z=0} \mathrm{d}x = 0. \tag{4b}$$

Furthermore, in the centre of the sample, $E = Bv|_{x=d/2} = Bv|_{z=w/2} \equiv 0$, so the second boundary condition is

$$E\big|_{x=d/2,z=w/2} = 0. \tag{5b}$$

The initial condition is still equation (6).

3.2.3. The V–I curve under an applied field. It is easy to see that for a non-linear $E(j)$ relationship such as the power-law form described by equation (2) with $n > 1$, the above boundary conditions will no longer be valid because there exist simultaneously applied and shielding currents in the sample, which will destroy the symmetric or anti-symmetric boundary conditions. Nevertheless, for $n = 1$, the linear case, the superposition principle is valid and one can deal with the applied current and magnetic field separately. Hence, the above boundary conditions are still correct. In our case, experiment shows that the value of n is not very large. Furthermore, what we are interested in is not the effect of the magnetic field but that of the geometric factor on the V–I curves. For these reasons we can still use the above boundary condition (4*a*).

3.3. Numerical method and results for a rectangular sample

3.3.1. Numerical method. To simplify the calculation, we first simplify the boundary condition (4*a*) and introduce a parameter q describing the aspect ratio of a sample which is defined as

$$q = \left[\int_0^w \left.\frac{\partial E}{\partial x}\right|_{x=0} \mathrm{d}z\right] \Big/ \left[-\frac{\mu_0}{2}\frac{\mathrm{d}I}{\mathrm{d}t}\right]. \tag{7a}$$

According to equation (4a) we have immediately

$$1 - q = \left[\int_0^d \left.\frac{\partial E}{\partial z}\right|_{z=0} \mathrm{d}x\right] \Big/ \left[-\frac{\mu_0}{2}\frac{\mathrm{d}I}{\mathrm{d}t}\right]. \tag{7b}$$

Now it is apparent for two special cases that

$q = 1/2$	$d/w = 1$	for a square cross section
$q = 1$	$d/w = 0$	for an infinite slab.

For a sample with rectangular cross section, we can assume that $0 < d \leqslant w$, i.e. $1/2 \leqslant q < 1$, without loss of generality, which means that the parameter q is connected with the aspect ratio of the rectangular sample. By combining equations (3), (4a), (5a), (6) and (7a), our simulation yields the electric field $E(x, z, t, q)$ as a function of q at any time before the sweep is stopped and at any position in the sample. According to equation (2), the corresponding current density $j(x, z, t, q)$ can then also be obtained. That is to say, we can calculate j and E at any time when a current is applied to a rectangular sample. Finally, the measurable voltage V and current I are obtained by integrating E and j, respectively.

3.3.2. Numerical results. First, we calculate the V–I characteristics of samples with the same area of cross section but different q, from

$$V = \frac{1}{wd}\int_0^l \mathrm{d}y \int_0^d \mathrm{d}x \int_0^w E(x, z, q)\,\mathrm{d}z \qquad I = \int_0^d \mathrm{d}x \int_0^w j(x, z, q)\,\mathrm{d}z.$$

Shown in figure 3 is the dependence of the V–I characteristic on q at zero applied field. It can be seen that there is no influence of the shielding current. Clearly, the V–I curve is shifted gradually toward the right (larger current) with increasing q, which means that the smaller d/w, the smaller the induced voltage V. To display in detail the dependence of the V–I curves on the aspect factor, we show in figure 4 the distribution of j in the x–z plane for different q with the same area and applied current I. The distribution of E has a similar shape and, for simplicity, is not shown here. It is seen that the aspect ratio strongly affects the distribution

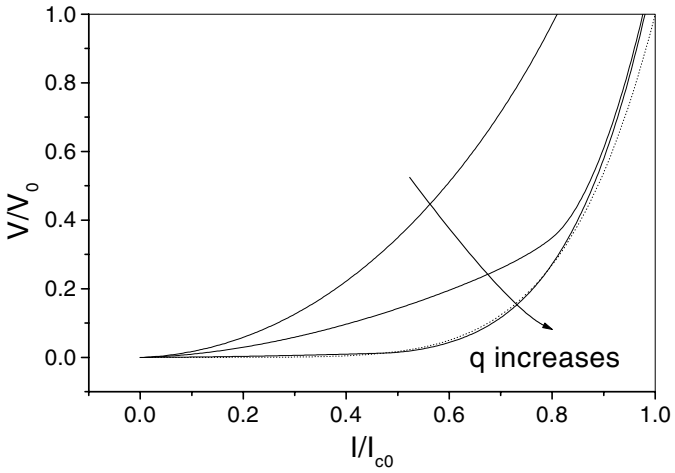

Figure 3. The effect of q on the V–I characteristics; q increases from 0.5 to 1, i.e. from a square cross section to an infinite slab. The E–j curve corresponding to the completely homogeneous case and described in equation (2) is also shown (dotted line) for comparison.

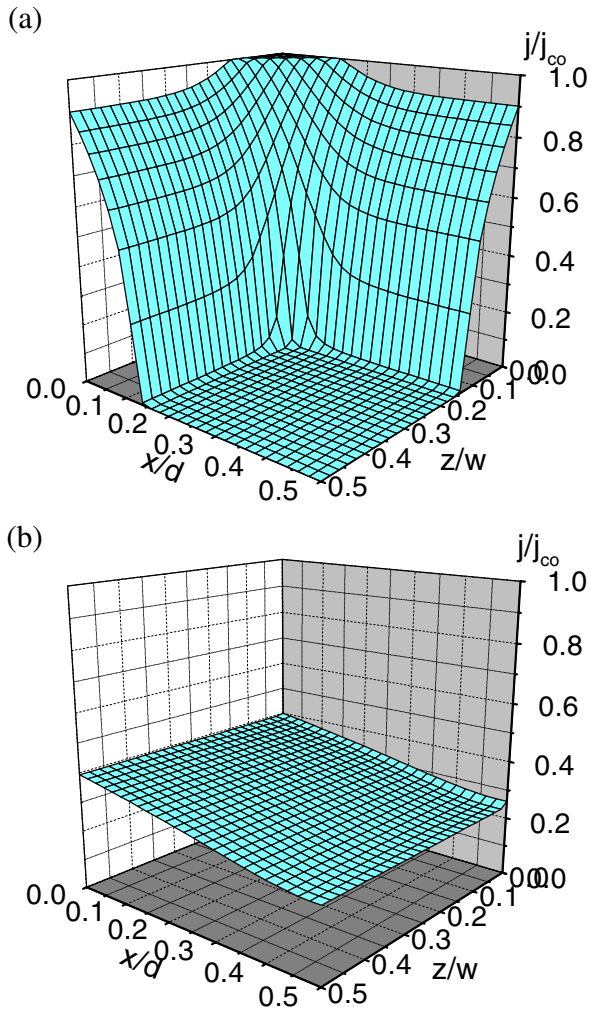

Figure 4. The effect of q on the distribution of the current density j in cross sections of the same area at zero field, $I = 0.3I_{c0}$, $\mathrm{d}I/\mathrm{d}t = (I_{c0}/300)\ \mathrm{s}^{-1}$ and $n = 6$. (a) $q = 0.5$. (b) $q \approx 1$.
(This figure is in colour only in the electronic version)

of the current and thus that of the electric field. Figure 4 demonstrates that the larger q, i.e. the thinner the sample, the more homogeneous the distributions of current. This result is understandable since the longest distance of flux diffusion is $d/2$ ($d < w$), and the larger q, the smaller d for the same cross section area (see figure 1)

Secondly, we simulate the temperature and field dependence of the V–I curves to compare with experimental values measured at different applied fields and temperatures. This will check our model in a specific case. For the Tl2212 bridge, the ratio $d/w = 0.2/30 = 1/150$ and $q \simeq 1$. The numerical V–I curves obtained by solving equation (3) are also shown in figure 2 to allow a fair comparison. We are confident that our numerical solution is correct in describing the rectangular diffusion of flux. The space and time evolution of j in the sample at a certain field and temperature is illustrated in figure 5, from which it can be seen that the current density j is indeed spatially homogeneous when the current is large enough, confirming equation ($2a$).

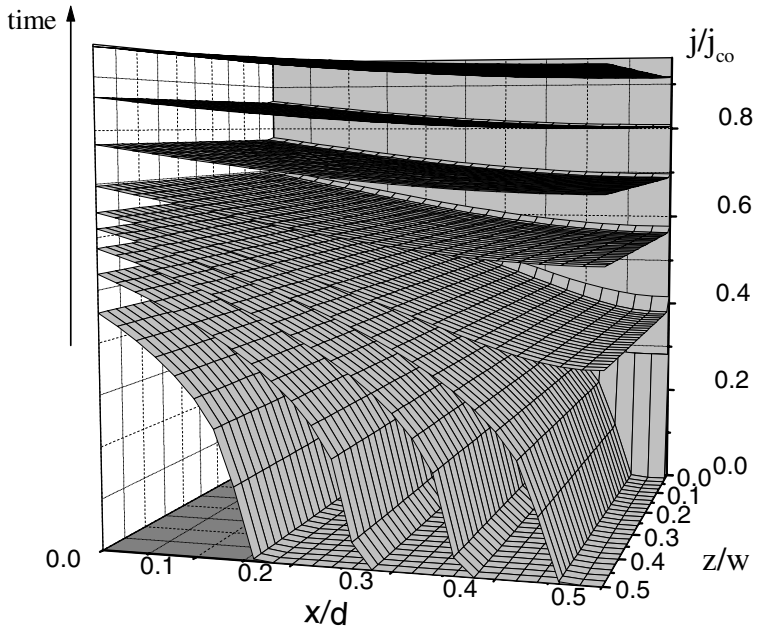

Figure 5. Space and time evolution of the current density j calculated with $d/w = 1/150$, $q \approx 1$, $\mathrm{d}I/\mathrm{d}t = (I_{c0}/200)\ \mathrm{s}^{-1}$, $T = 55$ K and $\mu_0 H = 0.507$ T. Arrows indicate the progress of the current-density profiles as the applied current is increased from $0.1I_{c0}$ to $0.9I_{c0}$. The corresponding V–I curve is shown in figure 2.

4. Summary

In summary, a simple numerical calculation procedure has been proposed which can solve the non-linear electric field diffusion equation, based upon the collective creep model. We have investigated the V–I curve of a sample with rectangular cross section at a certain sweep rate of the applied current. Calculating the spatial and time evolution of the electric field E and current density j underpinning the V–I curves, we show that the V–I curve shifts towards larger currents with decreasing sample thickness. To verify the proposed numerical procedure and the collective creep model on which the numerical observation was based, the V–I curves at different temperatures and fields for a $Tl_2Ba_2\ CaCu_2O_{8+x}$ (Tl2212) sample with rectangular cross section were measured and compared to the calculated curves. Comparison of the numerical and experimental results proves the validity of our simulation.

Acknowledgments

This work was supported by the Ministry of Science and Technology of China (NKBRSF-G1999-0646) and NNSFC under contract No 19994016.

References

[1] Campbell A M and Evetts E J 1972 *Adv. Phys.* **21** 199
[2] Iye Y, Tamegai T, Takeya H and Takei H 1987 *Japan. J. Appl. Phys.* **26** L1057
[3] Tinkham M 1988 *Phys. Rev. Lett.* **61** 1658
[4] Palstra T T M, Batlogg B, Van Dover R B, Schneemeyer L F and Waszczak J V 1990 *Phys. Rev.* B **42** 6621

[5] Worthington T K, Holtzberg F H and Feild C A 1990 *Cryogenics* **30** 417
[6] Charalambous M, Chaussy J and Lejay P 1992 *Phys. Rev.* B **45** 5091
[7] Safar H, Gammel P L, Huse D A, Bishop D J, Rice J P and Ginsberg D M 1992 *Phys. Rev. Lett.* **69** 824
[8] Kwok W K, Fleshler S, Welp U, Vinokur V M, Downey J, Crabtree G W and Miller M M 1992 *Phys. Rev. Lett.* **69**3370
[9] Zeldov E, Amer N M, Koren G, Gupta A, McElfresh M W and Gambino R J 1990 *Appl. Phys. Lett.* **56** 680
[10] Koch R H, Foglietti V, Gallagher W J, Koren G, Gupta A and Fisher M P A 1990 *Phys. Rev. Lett.* **64** 2586
Gammel P L, Schneemeyer L F and Bishop D J 1991 *Phys. Rev. Lett.* **66** 953
[11] Blatter G, Feigel'man M V, Geshkenbein V B, Larkin A I and Vinokur V M 1994 *Rev. Mod. Phys.* **66** 1125
[12] Ding S Y, Ren C, Yao X X, Sun Y and Zhang H 1998 *Cryogenics* **38** 809
[13] Ma L P, Li H C, Wang R L and Li L 1997 *Physica* C **279** 79
[14] Zeng Z Y, Yao X X, Qin M J, Ge Y, Ren C, Ding S Y, Ma L P, Li H C and Li L 1997 *Physica* C **291** 229
[15] Zhang P, Ren C, Ding S Y, Ding Q, Lin F Y, Zhang Y H, Luo H and Yao X X 1999 *Supercond. Sci. Technol.* **12** 571
[16] Gurevich A and Küpfer H 1993 *Phys. Rev.* B **48** 6477
[17] Gurevich A and Brandt E H 1994 *Phys. Rev. Lett.* **73** 178
[18] van der Beek C J, Geshkenbein V B and Vinokur V M 1993 *Phys. Rev.* B **48** 3393
[19] Brandt E H 1998 *Phys. Rev.* B **58** 6506
[20] Ding S Y, Ren C, Yi H J, Zeng Z Y, Yao X X, Fu Y X and Cai C B 1996 *Phys. Rev.* B **54** 16 211
[21] Malozemoff A P, Worthington T K, Yeshurun Y, Holtzberg F and Kes P H 1988 *Phys. Rev.* B **38** 7203
[22] Zeldov E, Clem J R, McElfresh M and Darwin M 1994 *Phys. Rev.* B **49** 9802
[23] Brandt E H 1994 *Phys. Rev.* B **49** 9204
[24] Brandt E H 1995 *Phys. Rev. Lett.* **74** 3025
Brandt E H 1995 *Phys. Rev.* B **52** 15 442
[25] Yan S L, Fang L, Song Q S, Yan J, Zhu Y P, Chen J H and Zhang Z B 1993 *Appl. Phys. Lett.* **63** 1845
[26] Abulafia Y, Shaulov A, Wolfus Y, Prozorov R, Burlachkov L, Yeshurun Y, Majer D, Zeldov E and Vinokur V M 1995 *Phys. Rev. Lett.* **75** 2404
[27] Abulafia Y, Shaulov A, Wolfus Y, Prozorov R, Burlachkov L, Yeshurun Y, Majer D, Zeldov E, Wühl H, Geshkenbein V B and Vinokur V M 1996 *Phys. Rev. Lett.* **77** 1596